DOI: 10.61782/fa.2025.0966

FORUM ACUSTICUM EURONOISE 2025

WALL PRESSURE FLUCTUATIONS AND IMPACT ON THE NOISE FROM DISTRIBUTED ELECTRIC PROPELLERS

Luana G. Stoica[1*] **Elisa de Paola**[1] **Giorgia Capobianchi**[1]
Alessandro Di Marco[1] **Roberto Camussi**[1]
[1] DICITA, University of Roma Tre, Roma, Italy

ABSTRACT

In the pursue of new urban air mobility solutions, the VENUS project served as a test bench for a real-world application of distributed electric propulsion aircraft. Experimental investigations were carried out on a wing model, equipped with three tractor propellers, derived from a realistic regional aircraft configuration inside an open jet acoustically treated wind tunnel. Wall pressure fluctuations induced by the multiple propeller configuration on the wing were investigated, in particular on the leading edge of the wing, on the flap, and inside the gap between the flap and the wing. Measurements of the acoustic footprint and of the polar directivity were carried out using three far-field microphone arrays. The parameters varied during the measurements included propeller blade pitch angle, flap deflection angle and wing angle of attack, as well as the distances between the propellers and with respect to the wing. The importance of the different generation mechanisms on the far-field noise and their dependency on the position along the wing and test parameters was assessed applying two-point statistics.

Keywords: *wall pressure fluctuations, DEP, propellers, wind tunnel.*

1. INTRODUCTION

In recent years we witnessed the increased popularity of the distributed electric propulsion (DEP) with a variety of new technologies and aircraft concepts being developed. DEP aircraft concepts feature multiple electric propulsors around an airframe and one or more independent electric generators or energy storage devices [1].

Experimental investigations using high resolution PIV, force and aeroacoustic measurements were carried out in [2] finding that the noise distribution for twin-rotor configurations is a function of azimuthal angle and separation distance. Systematic testing on different dual propeller configurations were conducted both numerically and experimentally in [3] in order to gain insight in the mutual interaction effect on thrust and noise levels. In these two latter papers, two-bladed propellers for UAV applications were considered. A benchmark experiment on wake-ingesting propellers is discussed in [4], including fluctuating pressure and aeroacoustic analysis.

Realistic wing models with multiple bladed propellers were investigated in three different EU funded projects. In [5] we find the results of the study of a wing model equipped with three propellers with three blades each, both in tractor and pusher configuration in the framework of the ARTEM project. The project ERaCLE was focused on the aeroacoustics of a wing model propelled by two five-bladed pusher propellers [6]. In the current paper, the experimental database of the VENUS project was investigated with a focus on the wall pressure fluctuation analysis, and its correlation to the emitted far-field noise.

2. EXPERIMENTAL SET-UP

The VENUS model is inspired by a short range regional aircraft, with each wing powered by three distributed propellers to be used mainly in take-off and landing. Each propeller is composed of four blades. The blade geometry and the propellers positions along the wing were op-

*__Corresponding author__: luana.stoica@uniroma3.it.

timized with aerodynamic and aeroacoustic constraints. The experimental set-up is described in detail in [7].

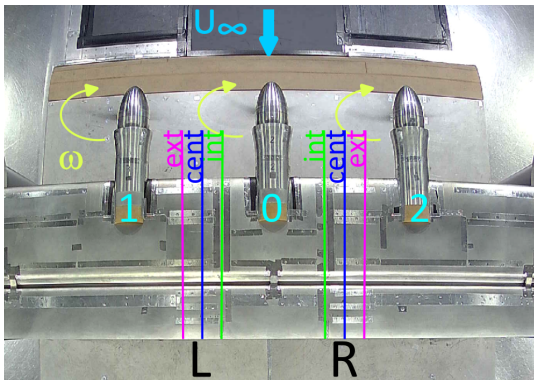

(a) Upper view model - pressure side wing

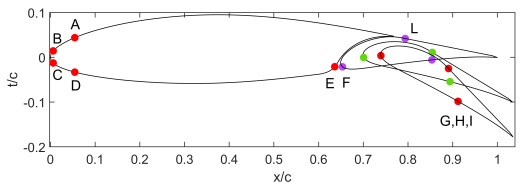

(b) Cross-section view

Figure 1: Fluctuating pressure sensors positions. The wing is seen from the pressure side.

A picture of the wing with the baseline DEP relative position and the position of the sensors is shown in Fig. 1 a, as seen from the pressure side of the wing, as the wing model was installed upside-down inside the wind tunnel. The unsteady pressure sensors (Knowles FG-23629-P16 capsule electret microphones) were installed on both sides of the central propeller, named left (L) and right (R) as seen when facing the flow, on three lines (internal, central and external with respect to the centre of the wing) with the aim of covering the interaction area between the propellers. Along the airfoil, the positions are marked with different letters and are mainly gathered around the leading edge, on the flap and in the gap between wing and flap. All the propellers spin counter-clockwise as seen from the flow, with a blade pitch angle of 17°. In the baseline position, the propeller blades are aligned on the same plane, at a distance from the wing of $0.52D$ and a hub to hub distance of $1.05D$. The wing chord is equal to $1.14D$. All the tested propellers positions can be found in Tab. 1. The wing is also equipped with a high lift device: the flap deflection angles are $\delta = 20°$ in take-off and $\delta = 35°$ in landing position. The wing pitch angle is set to 5° in both cases.

Table 1: Propellers' position in the DEP configurations tested.

	$\Delta Y/D$ 0-1, 0-2	$\Delta X/D$ 1, 2	$\Delta X/D$ 0
XY1	1.05	0.52	0.52
XY2	1.05	0.41	0.41
XY3	1.05	0.41	0.63
XY4	1.05	0.63	0.41
XY5	1.05	0.52	0.63
XY6	0.984	0.41	0.63
XY7	0.984	0.63	0.41

3. RESULTS AND DISCUSSION

The fluctuating pressure signals from the wall microphones on the wing are analysed in this section. The tests analysed herein are performed in take-off wing configuration (AoA=5°, flap deflection 20°) with all three propellers running in-phase at an advance ratio of $J = 0.654$. The Reynolds number of the incoming flow is $Re_\infty = 0.81 \cdot 10^6$, whereas for the propeller, $Re_{0.75} = 1.3 \cdot 10^5$, based on the propeller chord at the 75% propeller-blade station. The fluctuating pressure coefficient is defined as $c_{p,rms} = \frac{\sigma_p}{q}$, where σ_p is the standard deviation of the fluctuating pressure and q is the dynamic pressure measured in the wind tunnel test section.

An interesting feature is that sensors on the central lines show a notable difference in the spectra on both sides of the wing as we can see from the spectra measured in the baseline configuration in Fig. 2. We notice that the sensors on the external and internal lines of microphones exhibit tonal components up to around the 12th shaft frequency, whereas the central line of microphones exhibits an additional set of tonal spikes at higher frequency, in some cases up to the 36th BPF in some cases. This effect may be ascribable to the interaction between the vortices from the two adjacent propellers, and it is registered on both right and left side of the wing (see convention in Fig. 1). As the AoA is increased, this effect remains evident only on the pressure side of the wing, as probably

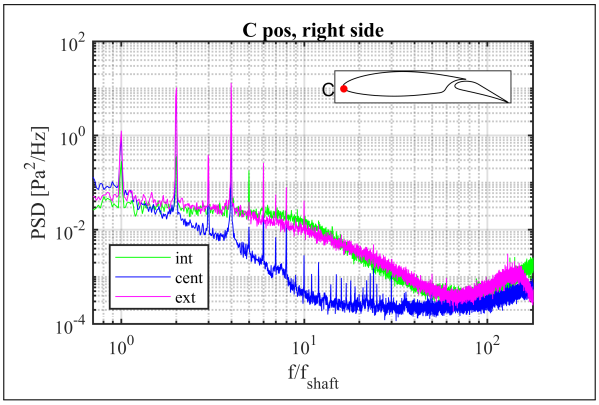

Figure 2: PSD of the fluctuating pressure from sensors in position C, right side of the wing - baseline.

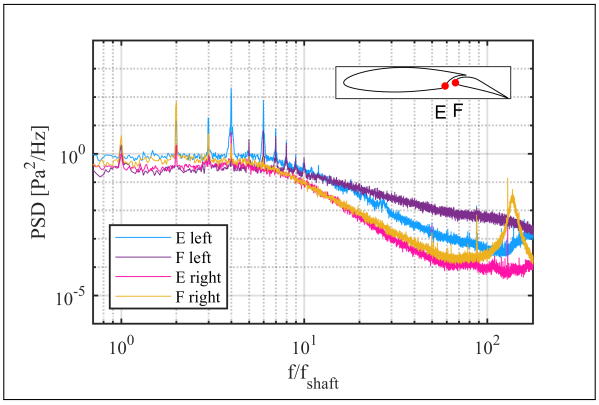

Figure 3: PSD of the fluctuating pressure from sensors in the gap between flap and wing - baseline.

the sensors on the upper side are screened by the airflow separating at the leading edge.

In Fig. 3, the spectra of the wall pressure in the gap between wing and flap are shown for the baseline configuration. These sensors are only installed on the line denoted as internal (green line in Fig. 1). On the right side of the wing, where we expect the disturbed wake of the central propeller to be impinging on the pressure side, the high frequency decay of the spectra has the same rate in E and F, around $f^{(-7/2)}$. On the left side of the wing, where the tip vortices from the central propeller are not impinging on these sensors, we have different features in the E and F positions. For the sensor E, we notice that the tone at the shaft frequency is not present, whereas the successive harmonics have a higher amplitude than in the F position.

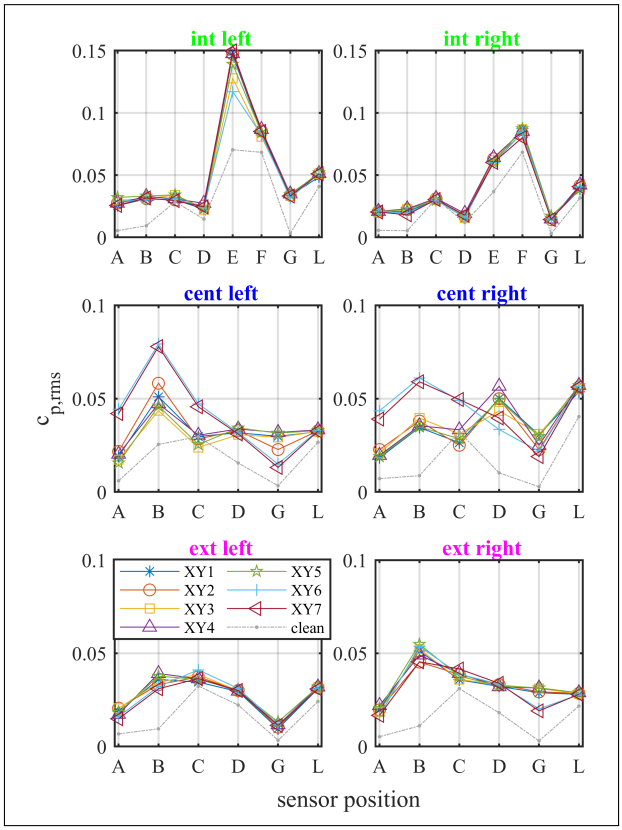

Figure 4: Trends of $c_{p,rms}$ along the wing model in different DEP configurations.

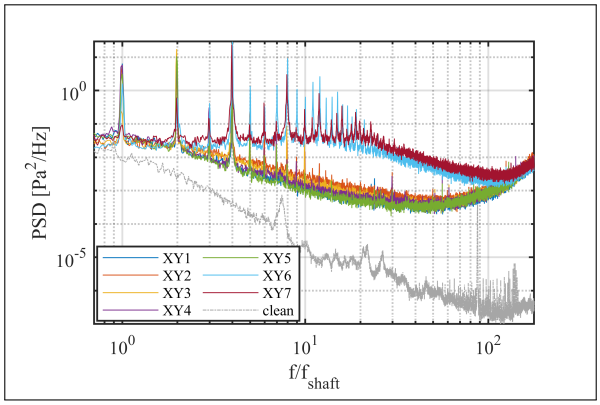

Figure 5: PSD of the fluctuating pressure from sensor B, central line, right side - DEP configuration effect.

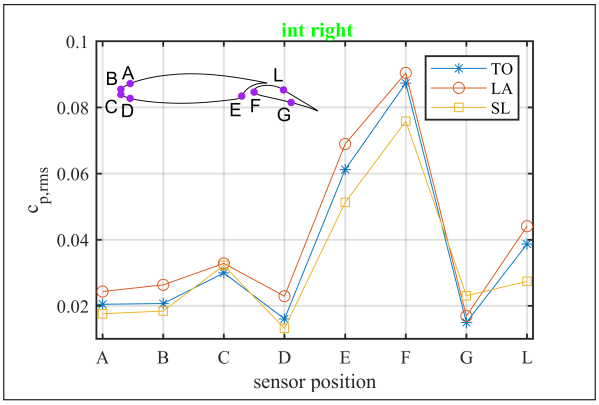

Figure 6: Trends of $c_{p,rms}$ along the wing model with different flap deflection angles.

Also the high frequency decay has a lower rate in F with respect to E, and in both cases is lower than the right side.

The effect of the different DEP configurations on the fluctuating pressure is investigated in Fig. 4, where also the results on the clean wing (i.e. without propeller blades) are included. Notable differences may be observed on the central lines of microphones, where the interaction between adjacent propellers is captured. In particular, configurations $XY6$ and $XY7$ exhibit the highest maximum value in position B and the lowest minimum in position G. This effect may be ascribed to the propellers planes overlapping or to the increased distance between the propellers axes. An intermediate value is found for position $XY2$, which has the three aligned propellers in their closest position with respect to the wing. The trends of the $c_{p,rms}$ on the external and internal lines are quite similar, with a local maximum on the leading edge, in position B or C depending on the line, and with another local maximum in position L on the upper side of the flap. The pressure fluctuations in the gap between the flap and the wing exhibit the highest values, with differences with respect to the other sensors up to 0.05 on the right side and up to 0.1 on the left side. This latter value may be be affected by the impinging wake from the propellers. Similar results are obtained in take-off and landing configurations.

In order to further investigate the origin of the maximum value of the fluctuating pressure, in Fig. 5, the spectra in position B from the central (blue) line on the right side of the wing are shown, for all the DEP configurations tested. The difference between the overlapping discs configurations and the others becomes obvious looking at the mid-high frequency part of the spectra, where a substantially higher level of energy is observed. The high frequency decay of the spectra from configurations XY6 and XY7 is approximately $f^{(-7/3)}$, typical value for the turbulent boundary layer acoustic-transition [8]. For the configurations with no overlap, the slope of the spectra decreases rapidly after the second shaft frequency.

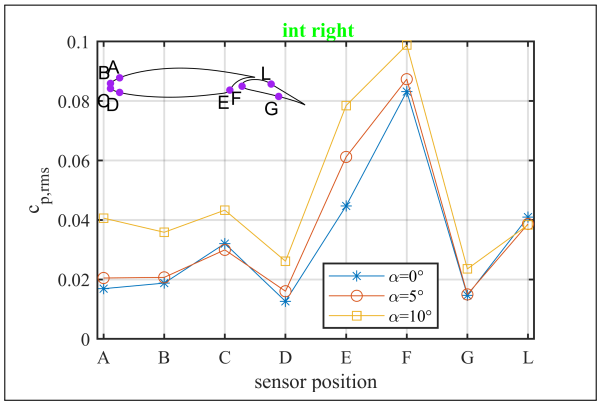

Figure 7: Trends of $c_{p,rms}$ along the wing model with different wing pitch angles.

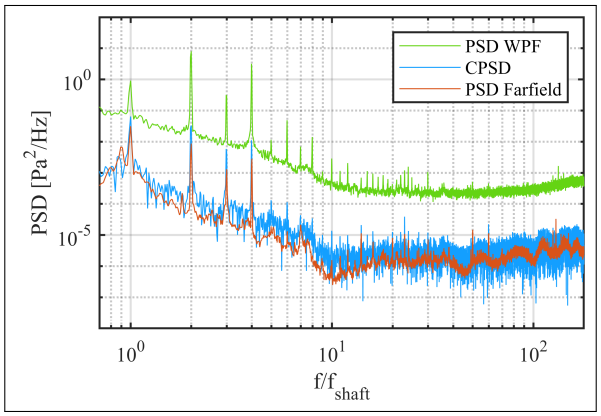

Figure 8: Comparison between PSD of the fluctuating pressure, farfield noise and cross-spectrum.

The effect of the flap deflection on the fluctuating pressure is shown in Fig. 6 for the baseline configuration in take-off, with the results from the sensors located along the internal line on the right side as an example. The landing configuration ($\delta = 35°$) exhibits the higher fluctuation, followed by the take-off and the side-line, with differences in the order of 0.005. This is especially true

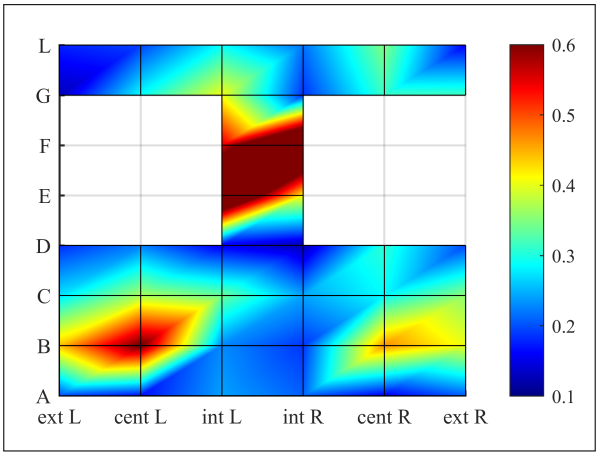

Figure 9: Covariance between the fluctuating pressure sensors and farfield noise.

for the sensors in the gap between the wing and the flap.

In Fig. 7, the results from the same sensors are plotted at different wing pitch angles. At $10°$, there is a $c_{p,rms}$ up to 0.02 higher, due to separation effects. For angles between $0°$ and $5°$ the values are similar, whereas for exceeding angles the fluctuations increase with the AoA, indicating a flow separation occurring. For the sensors in the gap between wing and flap the situation is different, with the fluctuations increasing with the AoA at all angles.

The cross-spectra were computed between the pressure sensors on the wing and one farfield sensor located at the centre of the acoustic footprint of the wing, near the propeller plane. An example is shown in Fig. 8, for the sensor in position C on the central line on the right side of the wing. The baseline configuration in take-off is considered. We can see a strong correlation on the first four shaft frequencies. The cross-spectrum also unveils the higher frequency tonal components which are more evident in the wall pressure spectra. The broadband component maintains the same shape as the far-field noise.

The covariance between the signals was then obtained integrating the cross-spectra, in order to understand which positions affect mostly the emitted noise (Fig. 9). The maximum correlation between the signals is found in the gap between the flap and the wing, although there are other areas concurring in a notable manner to the noise emission. In particular, we find a second maximum at the sensors in position B on the central lines, where the vortices from the adjacent propellers are interacting and impinging on the wing. In this position, flow separation may occur at the examined AoA of $5°$. A lower local maxima is also found at sensors in position C on the internal lines, which are closest to the central propeller. When comparing different flap positions, we find a higher correlation on sensors positions D and L when the flap is deflected with respect to the sideline configuration. As the the angle of attack is increased, the maximum correlation moves towards positions C and D on the left side of the wing, i.e. where the outflow from the propeller is impinging on the wing. Also the correlations measured on the flap in G and L increase with the AoA.

4. CONCLUSION

Wall pressure fluctuations on a DEP configuration were analysed in order to find the underlying mechanisms leading to noise generation. Signals are acquired from 44 fluctuating pressure sensors installed at different stations along the wing, surveying different areas on the airfoil, such as the leading edge of the wing, the gap between wing and flap and the flap.

The interaction between the adjacent propellers has a visible effect on the wall pressure fluctuations and is highly correlated with the acoustic footprint. Regarding the propellers relative position, the configurations with overlapping propellers discs and the greatest distance between their axes are responsible for the highest wall pressure fluctuations impinging on the wing. An influence of the flap deflection angle is also visible, with pressure fluctuations increasing with increasing deflection. The wing angle of attack is in its turn responsible for increasing the fluctuations, especially above $5°$, due to separation effects.

The cross-correlation between the wall pressure fluctuations on the wing and the farfield emitted noise was then examined. The highest correlation with the farfield noise is found in the gap between the wing and the flap, which is also responsible for the highest contribution to the pressure fluctuations on the wing. In addition, the points where the interacting tip vortices from the adjacent propellers are impinging on the wing are the second highest correlated with the acoustic footprint.

5. ACKNOWLEDGMENTS

This work is part of the project VENUS (inVestigation of distributEd propulsion Noise and its mitigation through wind tUnnel experiments and numerical Simulations), which has received funding from the Clean Sky 2 Joint

Undertaking under the European Union's Horizon 2020 research and innovation program under grant agreement 886019.

6. REFERENCES

[1] H. D. Kim, A. T. Perry, and P. J. Ansell, "A review of distributed electric propulsion concepts for air vehicle technology," in *AIAA/IEEE Electric Aircraft Technologies Symp. (EATS)*, pp. 1–21, IEEE, 2018.

[2] T. Zhou and R. Fattah, "Tonal noise acoustic interaction characteristics of multi-rotor vehicles," in *23rd AIAA/CEAS Aeroacoustics Conference*, p. 4054, 2017.

[3] H. Bu, H. Wu, C. Bertin, Y. Fang, and S. Zhong, "Aerodynamic and acoustic measurements of dual small-scale propellers," *Journal of Sound and Vibration*, vol. 511, p. 116330, 2021.

[4] K. Brown, J. Fleming, M. Langford, W. Walton, W. Ng, K. Schwartz, D. Wisda, and R. Burdisso, "Reduced-order prediction of unsteady propeller loading and noise from pylon wake ingestion," *AIAA Journal*, vol. 59, no. 9, pp. 3304–3316, 2021.

[5] J. Drofelnik, M. Andrejasic, B. Mocan, T. Kosel, *et al.*, "Measurement and modelling of aero-acoustic installation effects in tractor and pusher propeller architectures," in *AIAA AVIATION FORUM*, p. 2301, 2021.

[6] L. G. Stoica, S. Mancini, A. Di Marco, E. de Paola, R. Camussi, C. Aquilini, A. Kolb, and N. Paletta, "Experimental investigation and numerical modeling of noise generated by installed pusher propellers," *Journal of Aircraft*, vol. 0, no. 0, pp. 1–13, 0.

[7] E. De Paola, R. Camussi, G. Stoica, A. Di Marco, and G. Capobianchi, "Aerodynamic and aeroacoustic experimental investigation of a three propellers DEP configuration," *Aerospace Science and Technology*, vol. 154, p. 109508, 2024.

[8] M. K. Bull, "Wall-pressure fluctuations beneath turbulent boundary layers: some reflections on forty years of research," *Journal of Sound and Vibration*, vol. 190, no. 3, pp. 299–315, 1996.